Supplementary Information for

A Wire-Shaped Supercapacitor in Micrometer Size Based on Fe_3O_4 Nanosheet Arrays on Fe Wire

Guohong Li[1], Ruchun Li[2], Weijia Zhou[2,*]

[1]School of Chemistry and Pharmaceutical Engineering, QiLu University of Technology, Daxue Road, Western University Science Park, Jinan 250353, People's Republic of China

[2]New Energy Research Institute, School of Environment and Energy, South China University of Technology, Guangzhou Higher Education Mega Center, Guangzhou, Guangdong 510006, People's Republic of China

*Corresponding author. E-mail: eszhouwj@scut.edu.cn

1 Synthesis and Properties of MnO_2 on Carbon Fiber (CF@MnO_2) Positive Electrode Material

First, 5 cm of carbon fibers were immersed into a mixture of concentrated H_2SO_4 and HNO_3 (v: v=3:1), which was sonicated for 2 h to remove organic matter. The carbon fibers were then removed from the solution and washed with a copious amount of water, and dried in an electrical oven at 60 ℃ for 6 h. Typically, 2.5 mmol $KMnO_4$ and 1.0 mL HCl (36%) were dissolved in 20 mL deionized water to form a transparent solution. Then carbon fibers were transferred to a Teflon-lined stainless steel autoclave with the above solution and then heated in an electric oven at 140 ℃ for 12 h. Finally, the sample was removed out, washed with water and dried at 60 ℃ for 12 h.

In order to assemble asymmetric supercapacitor, MnO_2 nanosheets array were grown onto carbon fiber (CF@MnO_2), which used as contrast electrode. The SEM and TEM images are shown in Fig. S1, which possess nanowire structure. The XRD and XPS results also confirmed the successful synthesis of MnO_2 (Fig. S2). In addition, the electrochemical performance of the CF@MnO_2 was revealed in Fig. S3. The obtained CF@MnO_2 also possessed good capacitive properties (8.2 mF cm^{-1} at current of 0.8 mA) and cycling stability (71% capacitance retention after 5000 cycles).

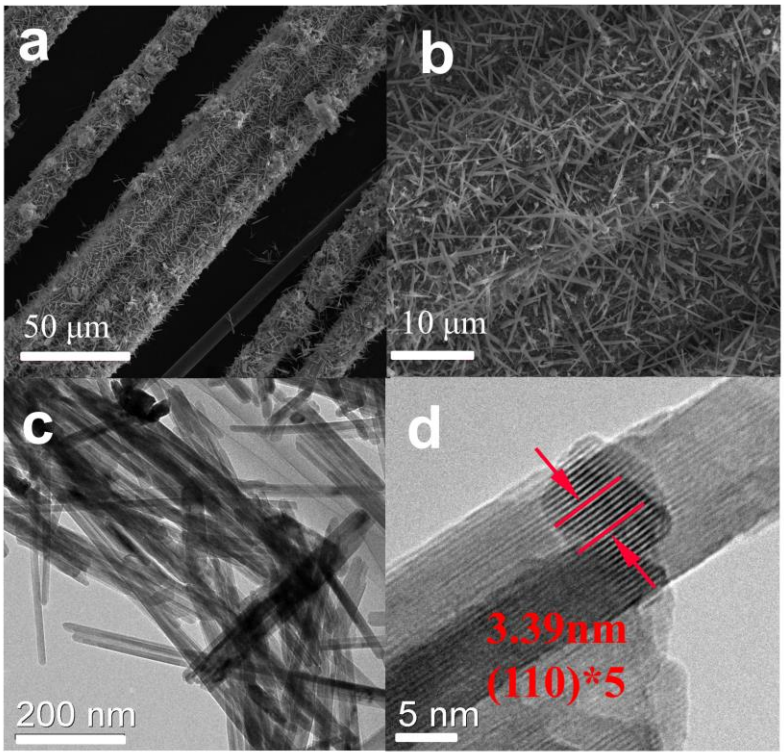

Fig. S1 a-b SEM images of the CF@MnO_2 at different magnifications. **c** Low and **d** HRTEM images of the MnO_2 (carefully scratched from CF@MnO_2).

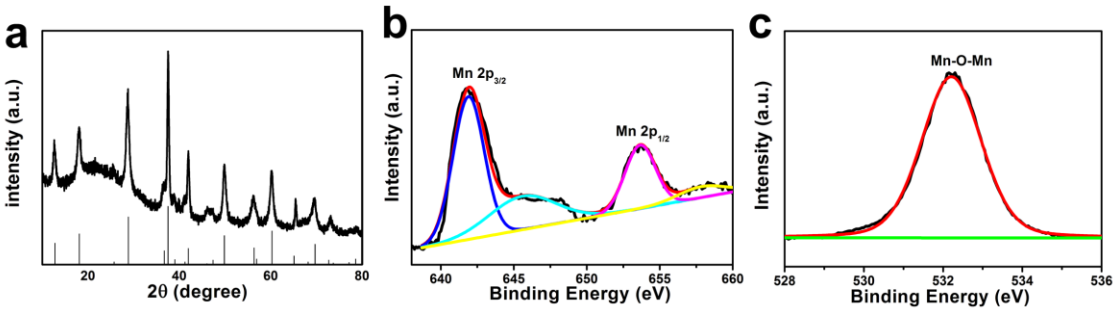

Fig. S2 a XRD patterns, high resolution XPS spectrum of **b** Mn 2p and **c** O 1s of the MnO_2 (carefully scratched from CF@MnO_2)

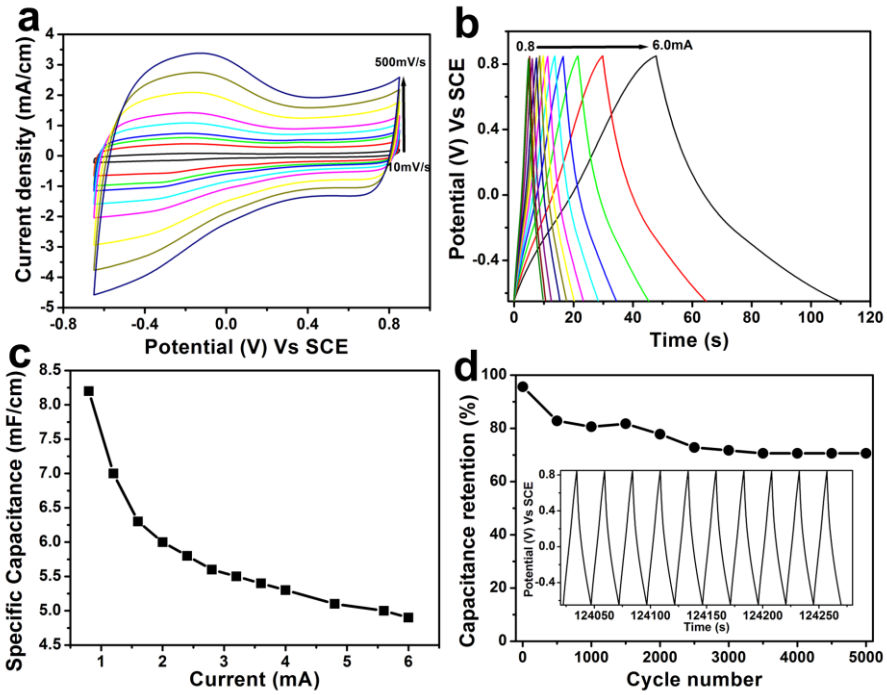

Fig. S3 a CVs of the CF@MnO_2 at different scan rates; **b** GCD curves of the CF@MnO_2 at different current. **c** Specific capacitances of the CF@MnO_2 as a function of current. **f** Cycling stability of the CF@MnO_2 electrode at a current of 2.4 mA; Inset is the last 10 charge/discharge profile of the CF@MnO_2.

2 Specific Capacitance Calculations

Specific capacitances (F cm^{-1}) were calculated from the CV (C_1) and charge–discharge curves (C_2) by Eq. S1 and S2, respectively, where I_1 (A) is the response current, ΔV (V) is the voltage window, v (V s^{-1}) is the scan rate, I_2 (A) is the constant discharge current, Δt (s) is the discharging time, and L (cm) is the length of the electrode.

$$C_1 = \frac{\int I_1 dV}{vL\Delta V} \quad \text{(S1)}$$

$$C_2 = \frac{I_2 \Delta t}{L\Delta V} \quad \text{(S2)}$$

Energy density (E) and power density (P) of the asymmetrical supercapacitor device were calculated by Eq. S3 and S4, respectively, where t (s) is the time for discharge.

$$E = \frac{1}{2}C(\Delta V)^2 \qquad \text{(S3)}$$

$$P = \frac{E}{\Delta t} \qquad \text{(S4)}$$

3 SEM images of $Fe@Fe_3O_4$ after oxidizing at different time

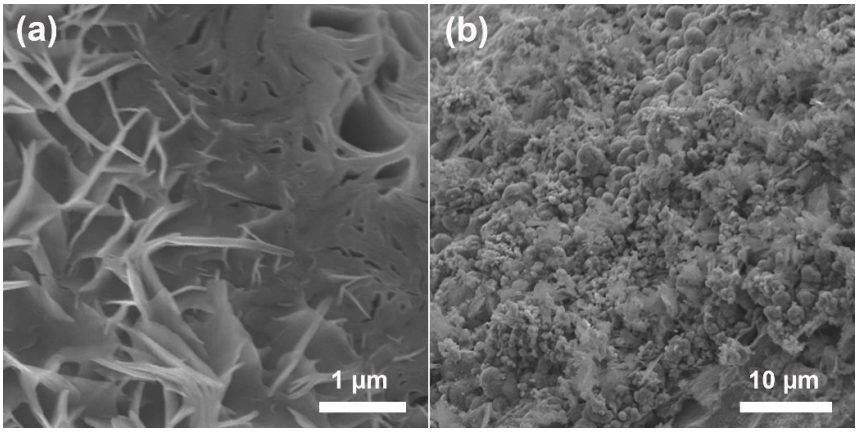

Fig. S4 the SEM images of **a** $Fe@Fe_3O_4$-20 and **b** $Fe@Fe_3O_4$-40

4 Raman Spectrum of Fe_3O_4

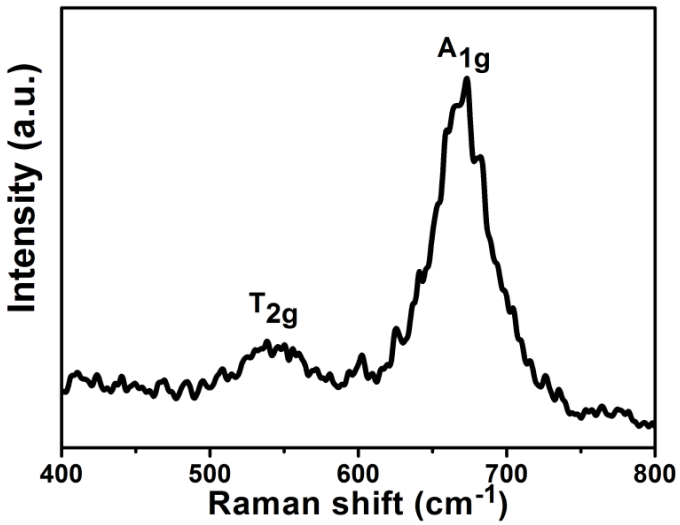

Figure S5 Raman spectrum of Fe_3O_4 scratched from $Fe@Fe_3O_4$.

5 XRD Patterns of Fe@Fe_3O_4 after oxidizing at different time

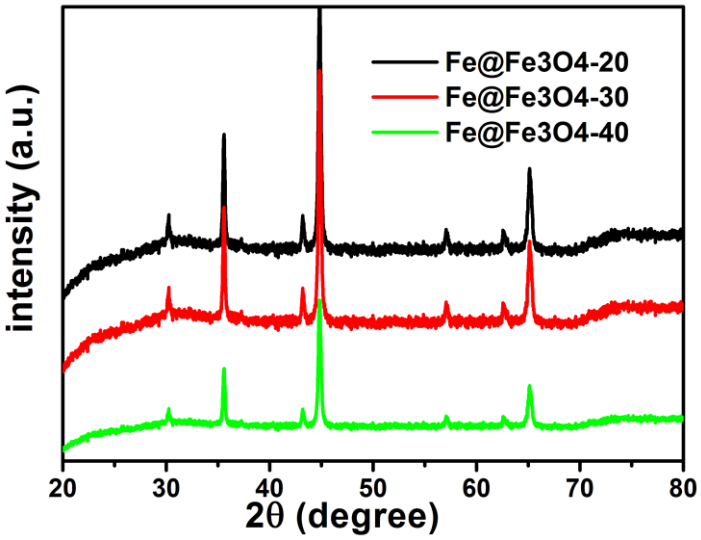

Fig. S6 XRD of Fe@Fe_3O_4-20, Fe@Fe_3O_4-30 and Fe@Fe_3O_4-40

The XRD patterns of Fe@Fe_3O_4-20, Fe@Fe_3O_4-30 and Fe@Fe_3O_4-40 was shown in Fig. S4. Except for two typical Fe substrate peaks at 2θ = 44.7° and 65.0°, all of peaks appeared at 30.2 °, 35.6 °, 43.2 °, 57.1 °, and 62.7 °agree well with the (220), (311), (400), (511), and (440) planes of Fe_3O_4 (JCPDS No. 75-0033), respectively, confirming the formation of Fe_3O_4. Compared with the XRD of samples, it is not obvious change with the increase of reaction time.

6 The Photo images of electrolyte after reaction at different time

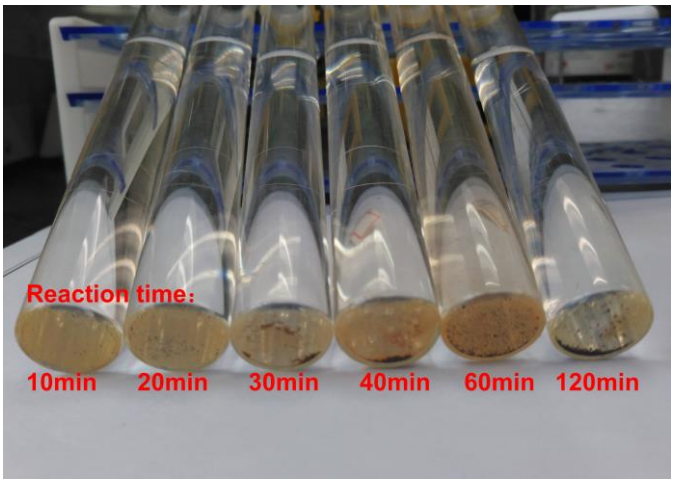

Fig. S7 The image of electrolyte after reaction. It can be seen that as-formed Fe_3O_4 was easy to fall out from Fe substrate, and more Fe_3O_4 precipitation was produced with increase of reaction time.

7 EIS plot of the Fe@Fe_3O_4-30

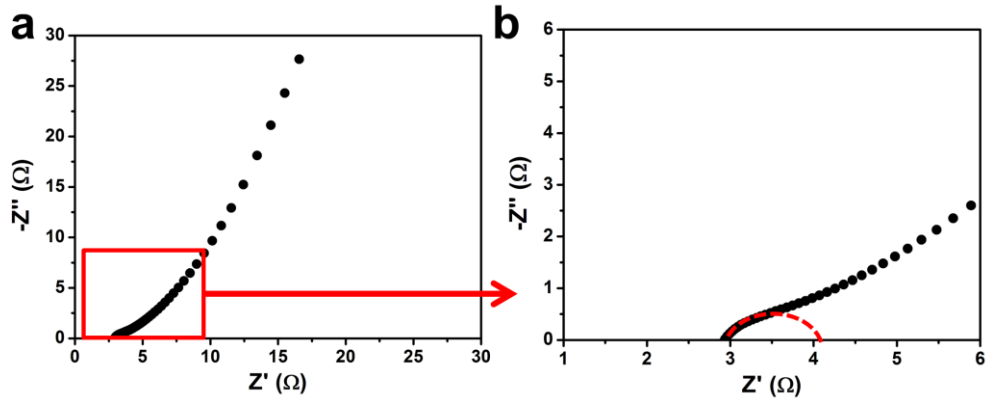

Fig. S8 EIS plot of the Fe@Fe_3O_4-30

The EIS measurements were carried out in the frequency range from 0.01 Hz to 100 kHz, as shown in Fig. S4. The curve consists of a semicircle in high frequency region and a straight line in low frequency region. The semicircle diameter reflects the charge transfer resistance, while the slope of straight line indicates the ion diffusion resistance. The Fe@Fe_3O_4-30 exhibits a smaller semicircle diameter only ~1.2 Ω and large slope, verifying a fast charge transfer kinetics and ion diffusion rate at the electrode/electrolyte interface. It is believed that the good charge transfer efficiency is helpful for the superior capacitive activity and cycling stability.

8 The capacity and stability of Fe@Fe_3O_4 under different oxidization time

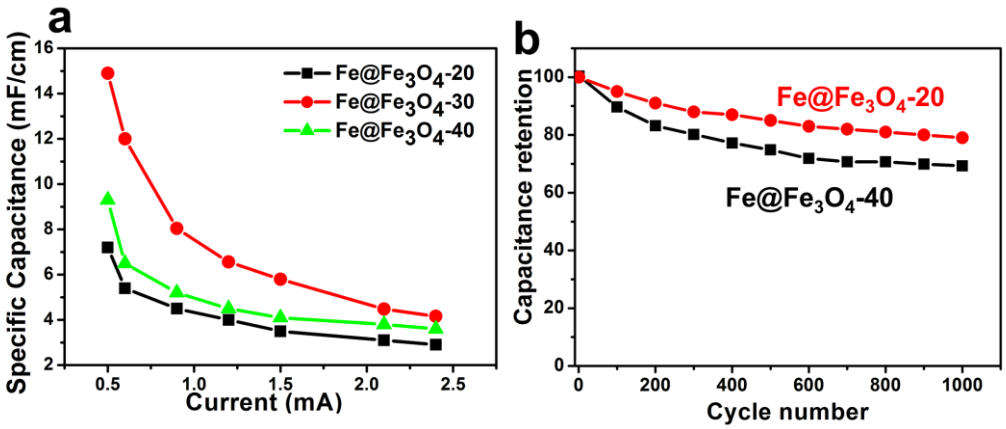

Fig. S9 The capacity **a** and stability **b** of Fe@Fe_3O_4-20 and Fe@Fe_3O_4-40

9 SEM Image of the Fe@Fe_3O_4-30 after the Cycle Test

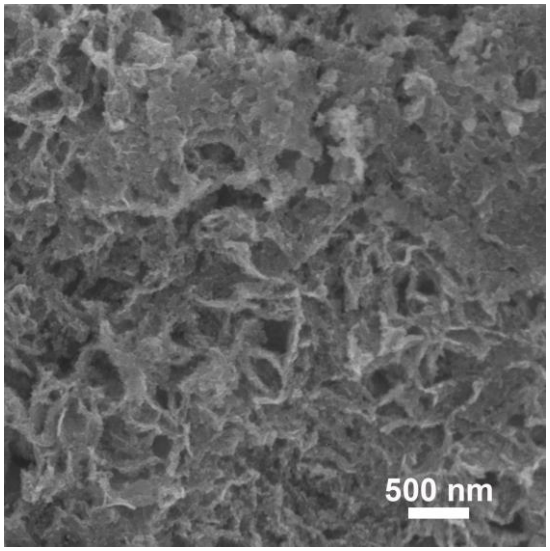

Fig. S10 the SEM image of the Fe@Fe_3O_4-30 after the cycle test

10 SEM Images of WSSC

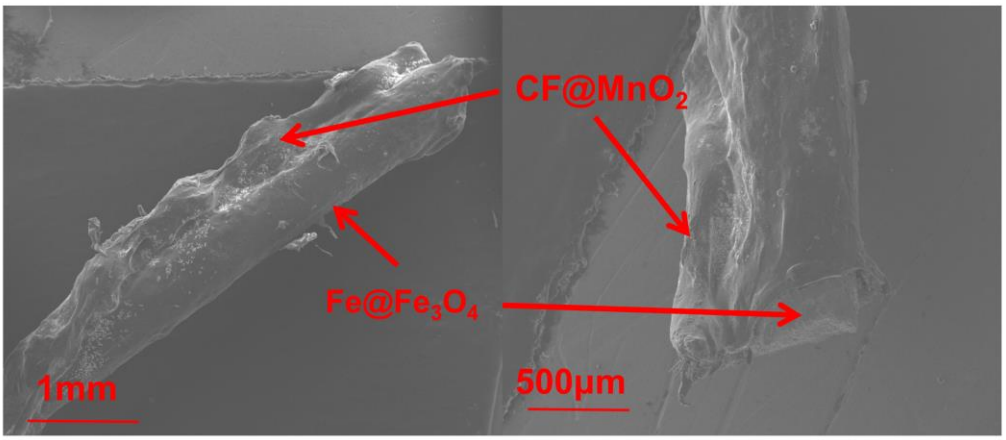

Fig. S11 the SEM image of wire-shaped all-solid-state asymmetric supercapacitor assembled by using Fe@Fe_3O_4-30 and CF@MnO_2

11 Weight of Fe_3O_4 under Different Oxidation Time

Table S1 The weight of Fe_3O_4

Samples	Weight before reaction (m_1, g)	Reaction time (min)	Weight after reaction (m_2, g)	Weight of Fe_3O_4 calculated by $[m_2-m_1]\times231.54\div64$
Fe wire	0.1468	0	0.1468	0
Fe@Fe_3O_4-10	0.1466	10	0.1507	0.01483
Fe@Fe_3O_4-20	0.1467	20	0.1524	0.02062
Fe@Fe_3O_4-30	0.1464	30	0.1537	0.02641
Fe@Fe_3O_4-40	0.1466	40	0.1541	0.02713
Fe@Fe_3O_4-60	0.1468	60	0.1536	0.0246
Fe@Fe_3O_4-120	0.1465	120	0.1529	0.02315